Proceedings of the ASME 2011 30th International Conference on Ocean, Offshore and Arctic Engineering
OMAE2011
June 19-24, 2011, Rotterdam, The Netherlands

OMAE2011-49010

EXPERIMENTAL STUDY ON VORTEX-INDUCED MOTIONS (VIM) OF A LARGE-VOLUME SEMI-SUBMERSIBLE PLATFORM

Rodolfo T. Gonçalves[1]
(rodolfo_tg@tpn.usp.br)

Guilherme F. Rosetti[1]
(guilherme.feitosa@tpn.usp.br)

André L. C. Fujarra[1]
(afujarra@usp.br)

Kazuo Nishimoto[1]
(knishimo@usp.br)

Allan C. Oliveira[2]
(allan_carre@petrobras.com.br)

[1]TPN – Numerical Offshore Tank
Department of Naval Architecture and Ocean Engineering, Escola Politécnica – University of São Paulo
São Paulo, SP, Brazil

[2]Research and Development Center (CENPES)
Petrobras
Rio de Janeiro, RJ, Brazil

ABSTRACT

A great deal of work has been developed on the spar and monocolumn vortex-induced motion (VIM) issue. However, there are very few published works concerning VIM of semi-submersible platforms, partly due to the fact that VIM studies for this type of platform recently became interesting particularly due to the increasing semi-submersible dimensions (columns diameter and height. In this context, a meticulous experimental study on VIM for this type of platform concept is presented here. Model test experiments were performed to check the influence of many factors on VIM, such as different headings and hull appendages. The results comply with in-line, cross-flow and yaw motion amplitudes, as well as with combined motions in the XY plane.

Keywords: vortex-induced motions (VIM), semi-submersible, model tests, 6DOF, coupled motion

1. INTRODUCTION

The study of VIM on semi-submersibles is more recent than on cylindrical platforms (such as monocolumns and spars). This fact is due to the current dimensions of the new semi-submersible platforms (better known as deep draft, see Rijken & Leverette (2008)) which have increased significantly, therefore promoting a notable VIM.

The main issue for the designers of risers and mooring lines is the direct relationship between the amplitude characteristics of VIM and the dimensions of the columns of the deep-draft semi-submersible units, according to which, the fatigue life of the SCR (steel catenary risers) can be reduced by 50% near the TDP (touch down point), as presented in Xiang, *et al*. (2010).

The geometry of the semi-submersible platforms implies a more complex VIM phenomenon than that identified for single cylindrical structures. In the case of semi-submersible platforms, the vortex shedding occurs around each column and thus the wake interference, different for each current incidence (platform heading), characterizes the VIM of the unit.

In this scenario, experimental works on VIM of semi-submersible platforms were presented by Rijken, *et al.* (2004); Waals, *et al.* (2007); Rijken & Leverette (2008) and Hong, *et al.* (2008); Stansberg (2008) also verified VIM on semi-submersible. In another work, Rijken & Leverette (2009) showed field measurements of VIM phenomenon in a deep-draft semi-submersible. Recently, Xiang, *et al.* (2010) estimated the damage caused by the VIM in the fatigue life of risers and mooring systems, for the same type of platform.

This study aims to experimentally demonstrate the presence of VIM on a semi-submersible platform to be operated by Petrobras-BR and at the same time to verify two important issues of the phenomena, which are: the relative position between the columns and the current direction and the hull appendages position. These two aspects have a great influence on the vortex shedding due to wake interference, as can be seen as follows.

2. EXPERIMENTAL SETUP

The experimental setup is characterized by a small-scale model of the semi-submersible unit, see Figure 1, supported by a set of equivalent horizontal moorings, see Figure 2, in the towing tank at the Institute of Technological Research (IPT) in São Paulo, Brazil. The adopted scale was 1:100. Only the hydrodynamic important appendages were represented, see Figure 3, as:

- The riser supports, located at the pontoons, see details in Figure 3 and Figure 4;
- The fairleads and the mooring stretches, located vertically at the external column faces, see details in Figure 3 and Figure 5;
- The hard pipes, located vertically at the internal column faces, see details in Figure 3 and Figure 6.

Figure 1 – Picture of the semi-submersible model scaled in 1:100.

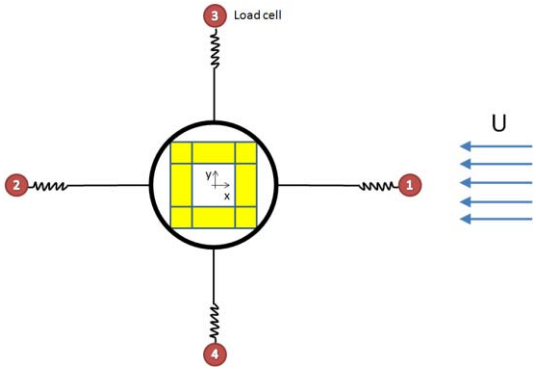

Figure 2 – Sketch of the equivalent mooring system composed of four lines.

Figure 1 presents details of the semi-submersible small-scale model. It was built with a ring located in the column portions above the water level to fix the equivalent mooring system, as can be seen in Figure 2. That ring allowed the use of the same mooring configuration for all different current incidences, i.e. the same value of mooring stiffness.

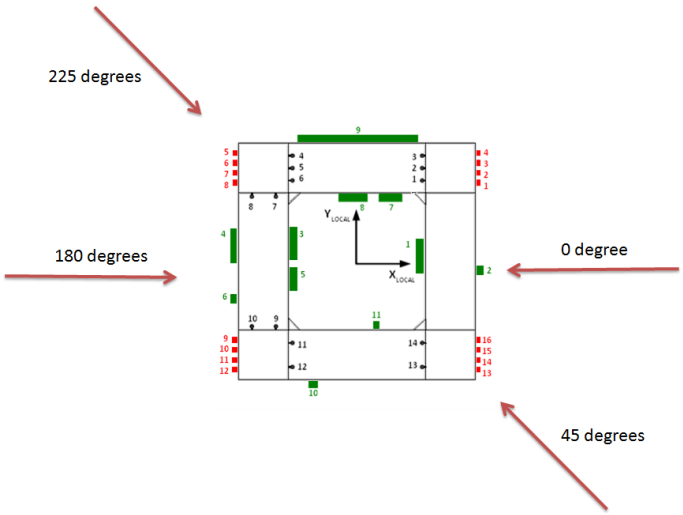

Figure 3 – Top view of the semi-submersible model showing the definition of incidence angles and hull appendages position. The riser supports, the fairleads and the hard pipes are represented in green, red and black color, respectively.

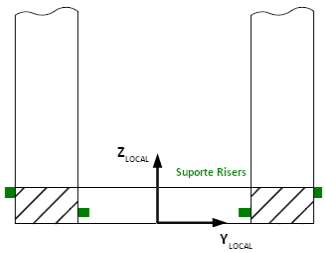

Figure 4 – Front view of the semi-submersible model showing the riser supports position, in green.

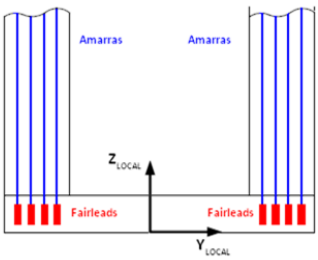

Figure 5 – Front view of the semi-submersible model showing the position of fairleads and mooring lines, in red and blue, respectively.

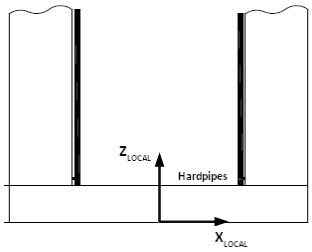

Figure 6 – Front view of the semi-submersible model showing the hard pipes position, in black.

The current incidences tested were: 0, 15, 30, 45, 180, 195, 210 and 225 degrees. The angles were defined according to Figure 3. At least 18 different reduced velocities were tested for each condition.

The analysis methodology for defining characteristics amplitudes motions (transverse, in-line and yaw) are described in the next section.

3. ANALISYS METHODOLOGY

The experimental results of the VIM on the small-scale model of the semi-submersible platform were analyzed by means of the HHT method, as presented in Gonçalves, *et al.* (2010a) and Gonçalves, *et al.* (2010b). The procedure is summarized as follows.

The HHT was developed by Huang, *et al.* (1998) as an alternative to deal with non-stationary signals that arise from non-linear systems. This analysis applies the typical Hilbert transform to a finite set of 'Intrinsic Mode Functions' (IMFs), which are obtained from the original signal through an 'Empirical Mode Decomposition' (EMD). The EMD method is based on a recursive subtraction of successively calculated mean between the two time-envelope of extrema contained in the signal (maxima and minima), which are then spline fitted. Such a recursive procedure is carried out for each IMF limited by a standard deviation stopping condition that is applied at each step. The IMF set is complete by construction.

Considering $Z_j(t)$ as an analytic function, for example, one of the IMFs is defined as follows:

$$Z_j(t) = X_j(t) + iY_j(t) = a_j(t)\exp\left[i\theta_j(t)\right] \quad (1)$$

The real part,$X_j(t)$ is the proper IMF and the complex part is the Hilbert Transform of $X_j(t)$, with P standing for principal value.

$$Y_j(t) = \frac{1}{\pi} P \int_{-\infty}^{+\infty} \frac{X_j(\tau)}{t-\tau} d\tau \quad (2)$$

Accordingly, the original signal can be decomposed into the IMF set, as in a 'generalized Fourier series':

$$X(t) = Re\sum_{j=1}^{n} a_j(t)\exp\left[i\int \omega_j(t)dt\right] \quad (3)$$

$$\omega_j(t) = \frac{d}{dt}\left[\theta_j(t)\right] \quad (4)$$

Where not only the amplitude $a_j(t)$ but also the local phase $\theta_j(t)$ and thus the local (or instantaneous) frequency $\omega_j(t)$ of each IMF are time dependent, this one formalized through the stationary phase method, as pointed out in Huang, *et al.* (1998).

By performing this analysis, the amplitude and the instantaneous frequency can be presented as functions of time in a three-dimensional plot, the so-called Hilbert spectrum, $H(\omega, t)$. Consequently, the HHT is extremely indicated for amplitude and frequency modulation, characteristics frequently found in VIM signals. Moreover, the distribution of energy is more accurately performed as energy can be locally concentrated in a range of frequencies and not all along.

As VIM signals can be rather non-stationary, it is also difficult to define the amplitude of the signal by usual analysis. This is another issue that HHT can resolve as local amplitude is obtained regardless of the non-stationary behavior.

A time history of a typically VIM signal in the transverse direction has few peaks in the signal (for example, 30 peaks including maxima and minima) which may give rise to poor statistic characteristics for the evaluation of the characteristic amplitude in the transverse direction as a mean of 20% highest peaks, i.e. mean of only 6 points.

The non-dimensional amplitude was based on a work by Gonçalves, *et al.* (2010a) and can be defined by taking the mean of the 10% largest amplitudes as obtained in the HHT, both for motion in the transverse and in-line directions, and the yaw motion. In the HHT, the amplitude is time function, then the mean of the 10% largest amplitudes is proportional to the length of data and the sampling frequency, i.e. mean of around 400 points (considering a length data of 400s and sample frequency equal to 10Hz).

The reduced velocity is defined as

$$V_r = (U.T_0)/D \quad (5)$$

where U is the incident current velocity, T_0 is the natural period of motion in the transverse direction in still water and D is the characteristic length of the section of the body subjected to a vortex shedding. In the case of VIM of semi-submersible, the value D can be written as a function of the current incidence angle, in order to better represent the characteristic length of the column section on the flow, i.e.:

$$D = L(|sen\emptyset| + |cos\emptyset|) \quad (6)$$

where L is the face dimension of the column and $\emptyset$ is the incident current angle. Details of the nomenclature and definitions can be seen in Figure 7.

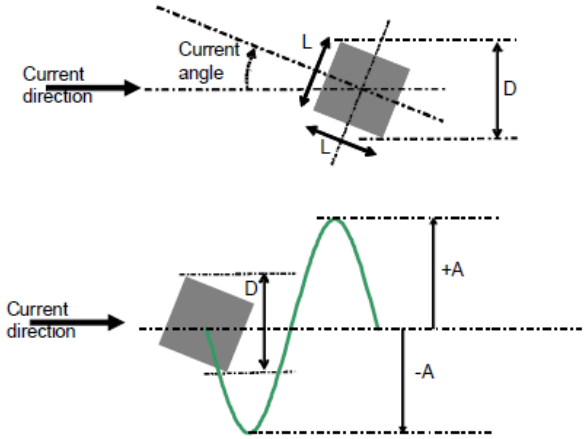

Figure 7 – Definition of parameters A (amplitude characteristic), D (projected length) and L (column dimension). Source: Rijken & Leverette (2008).

The motion characteristic amplitudes in the transverse and in-line direction are nondimensionalized by the dimension L, i.e. is the same value for all incidence conditions. This choice permits to directly compare results from different incidence conditions.

4. EXPERIMENTAL RESULTS

4.1. Motions in the Transverse Direction

Respectively, Figure 8 and Figure 9 present the results of nondimensional characteristic amplitude for motion in the transverse direction at 0, 15, 30, 45 degrees incidence, and 180, 195, 210,225 degrees incidence.

According to those results, the 30, 45, 210 and 225 degrees showed the largest VIM amplitudes in the transverse direction. The values obtained were around $A_y/L \cong 0.4$ for $7.0 \leq Vr \leq 8.0$.

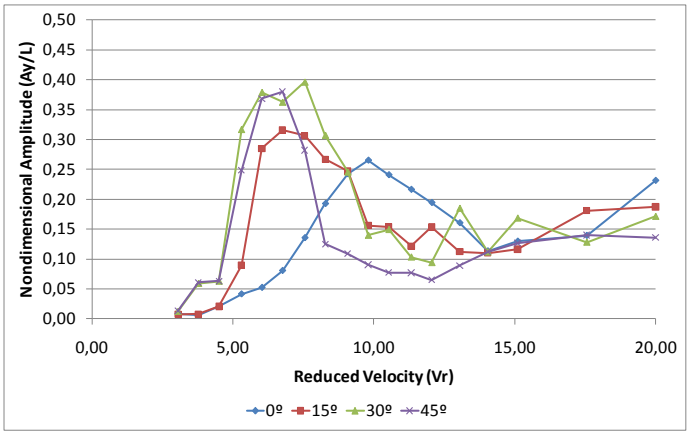

Figure 8 – Nondimensional amplitudes for the motions in the transverse direction for different current incidences: 0, 15, 30 and 45 degrees.

Additionally, the largest amplitude values for 15 and 195 degrees incidence occur at the same range of $7.0 \leq Vr \leq 8.0$ but with a reduced value of $A_y/L \cong 0.3$.

Except for the 0 and 180 degrees incidence, all other incidences showed a range of synchronization at reduced velocity greater than 4.0 and less than about 14.0.

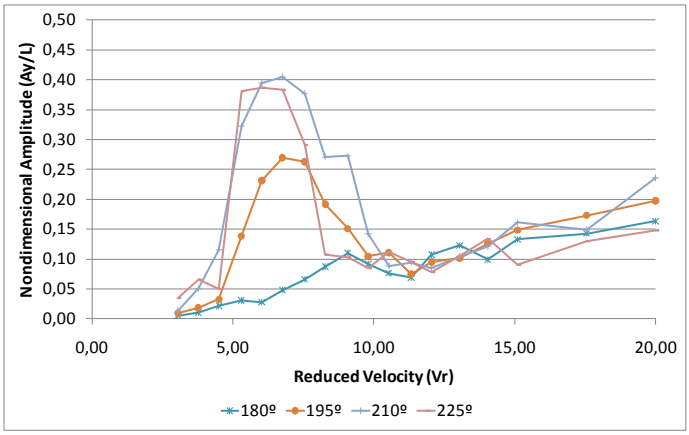

Figure 9 – Nondimensional amplitudes for the motions in the transverse direction for different current incidences: 180, 195, 210 and 225 degrees.

It is important to highlight that for $V_r > 14$, it is not possible to define one oscillation frequency, thus the small motion amplitudes. In this region, there is no synchronization between the vortex shedding and the natural period of the motion in the transverse direction, and then there is no pronounced VIM.

Figure 10 to Figure 13 help to better understand the appendages influence on VIM for each current incidence.

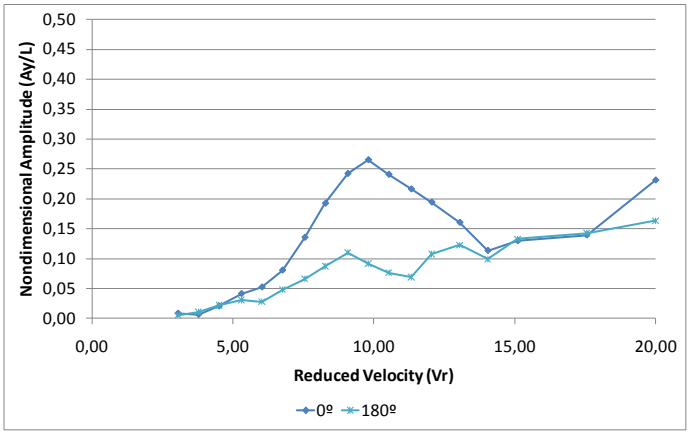

Figure 10 – Nondimensional amplitudes for the motions in the transverse direction for different current incidences: 0 and 180 degrees.

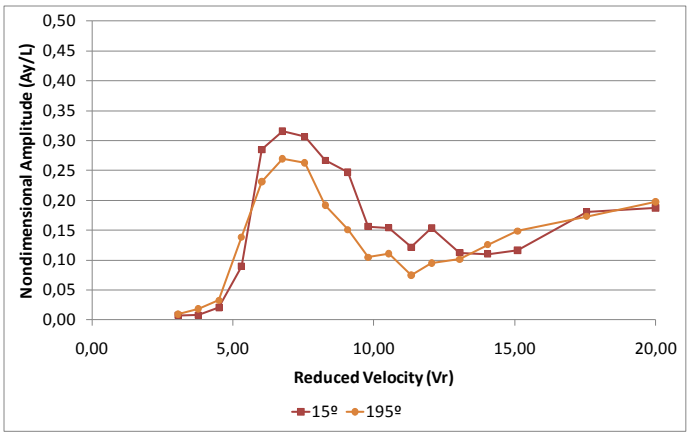

Figure 11 – Nondimensional amplitudes for the motions in the transverse direction for different current incidences: 15 and 195 degrees.

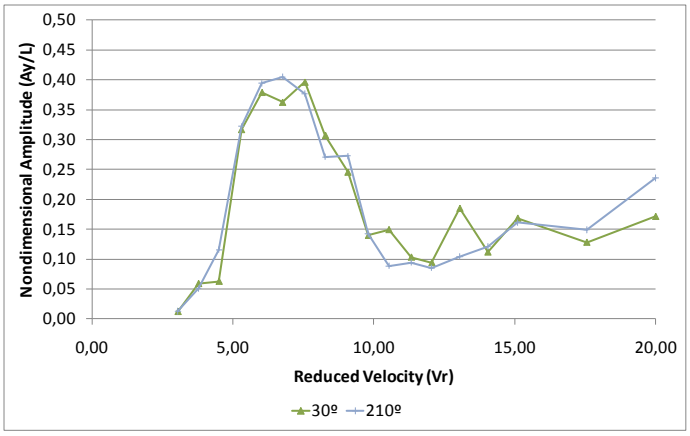

Figure 12 – Nondimensional amplitudes for the motions in the transverse direction for different current incidences: 30 and 210 degrees.

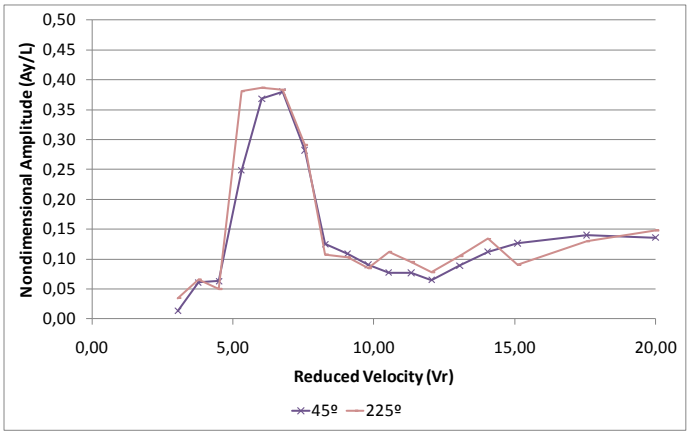

Figure 13 – Nondimensional amplitudes for the motions in the transverse direction for different current incidences: 45 and 225 degrees.

According to Figure 10, the asymmetry caused by the appendages is more pronounced for 0 and 180 degrees incidence. This difference may be attributed to the presence and position of the hard pipes in the 180 degrees incidence, see details in Figure 3, that promote a great modification in the wakes and consequently a loss in the shedding synchronization, which implies reduced motions in the transverse direction. For 0 degree incidence, the hard pipes are immersed in the wakes, which do not influence the vortex shedding, which implies motions in the transverse direction larger than those for 180 degrees incidence. The same asymmetry promoted by the presence of hard pipes can also be illustrated by comparing the 15 and 195 degrees incidence in Figure 11.

The other current incidences 30 and 210 degrees, and 45 and 225 degrees, see Figure 12 and Figure 13, respectively, did not show any influence due the asymmetry of the appendages.

4.2. Motions in the In-Line Direction

Figure 14 presents the results of nondimensional characteristic amplitudes for the motion in the in-line direction at 0, 15, 30, 45, 180, 195, 210 and 225 degree incidences.

According these results, the 15, 30, 195 and 210 degree incidences showed the largest VIM amplitudes in the in-line direction. The values obtained were around $A_x/L \cong 0.15$ for $6.0 \leq Vr \leq 8.0$.

The motions in the in-line direction showed to be non-periodic for $Vr \geq 10.0$, as a consequence, the values of A_x/L are very difficult to determine.

A little difference in the in-line motion dues to the asymmetry of the hull appendages cannot be seen, except for the 45 and 225 degrees incidence.

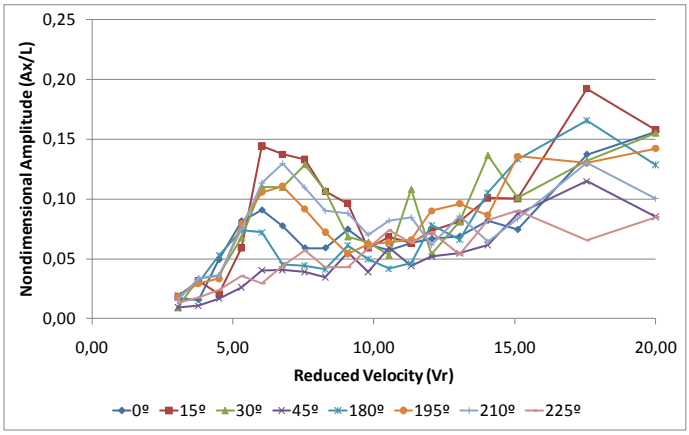

Figure 14 – Nondimensional amplitudes for the motions in the in-line direction for different current incidences: 0, 15, 30, 45, 180, 195, 210 and 225 degrees.

4.3. Yaw Motions

Respectively, Figure 15 and Figure 16 present the results of yaw characteristic amplitudes for 0, 15, 30 and 45 degree incidences, and 180, 195, 210 and 225 degree incidences. According to those figures, a synchronization regime of the yaw can be identified. Waals, *et al.* (2007) also identified

considerable values of yaw motions in their experiments with some type of semi-submersible platforms, but concluded that the yaw was observed as a consequence of a galloping phenomenon.

The results presented herein suggest the existence of vortex induced yaw motion (VIY). This phenomenon occurs when the vortex shedding frequency, deriving from columns interference, gets similar to the natural frequency of yaw motion of the semi-submersible. The following results corroborate the existence of a lock-in for yaw oscillations.

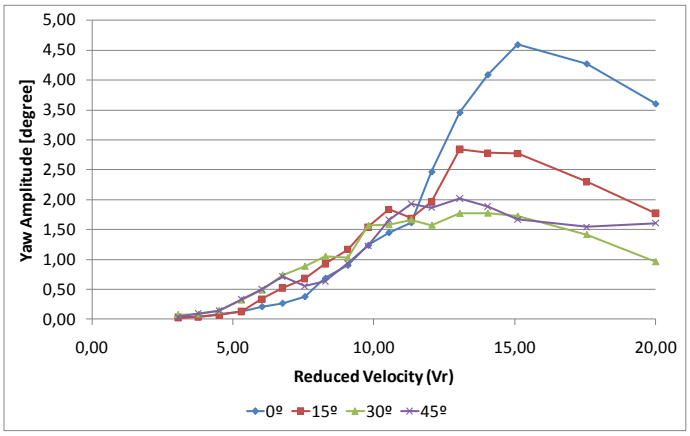

Figure 15 – Yaw characteristic amplitudes for different current incidences: 0, 15, 30 and 45 degrees.

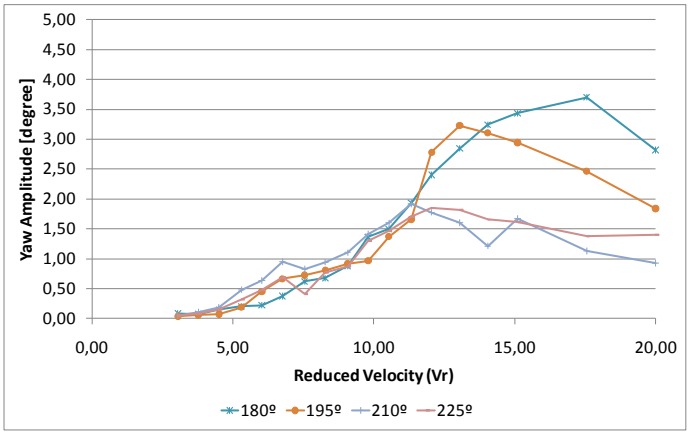

Figure 16 – Yaw characteristic amplitudes for different current incidences: 180, 195, 210 and 225 degrees.

The lock-in for the yaw motions, see Figure 15 and Figure 16, are presented for a range of $14.0 \leq Vr \leq 16.0$ differently for motions in the transverse direction in which the lock-in range is $5.0 \leq Vr \leq 10.0$. This fact is due to the larger natural frequency for yaw motions than the transverse ones, which implies larger current velocity to evidence the lock-in for yaw motions.

The influences of the hull appendages in the yaw motion are presented in Figure 17 to Figure 20. It is possible to verify, in Figure 17, the largest yaw amplitudes $A \cong 4.5$ for 0 and 180 degree incidences. Moreover, only in those current incidences is it possible to see the influence of the asymmetry of the hull appendages.

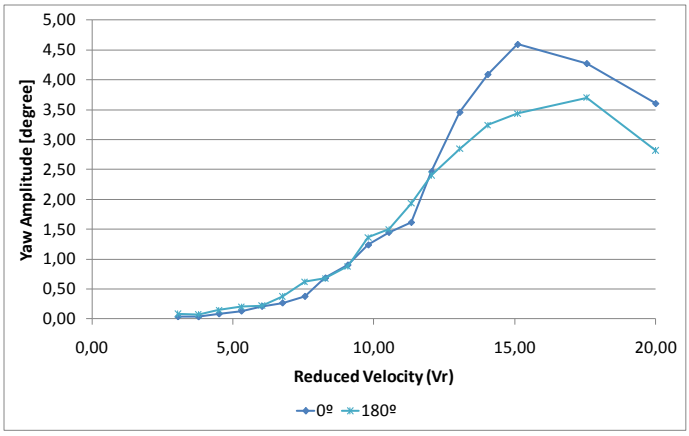

Figure 17 – Yaw characteristic amplitudes for different current incidences: 0 and 180 degrees.

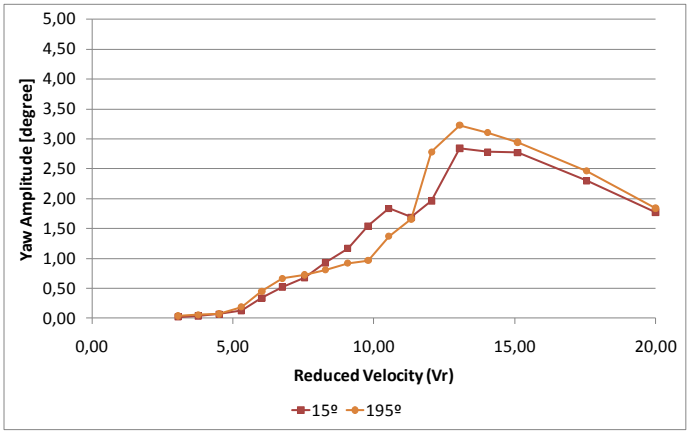

Figure 18 – Yaw characteristic amplitudes for different current incidences: 15 and 195 degrees.

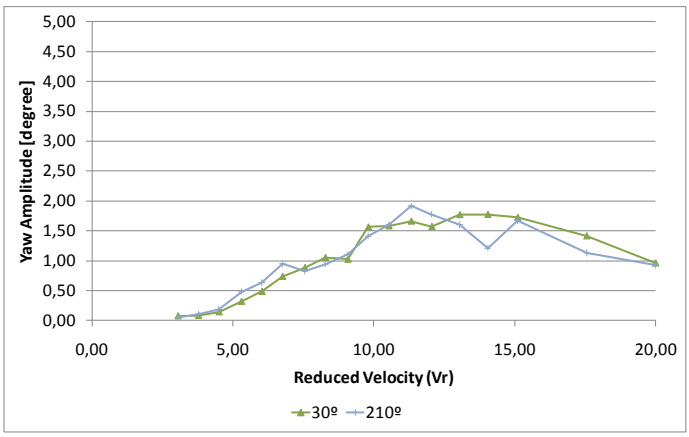

Figure 19 – Yaw characteristic amplitudes for different current incidences: 30 and 210 degrees.

The reduced velocities for yaw motions were re-calculated using the yaw natural period in still waters, T_6, to confirm the

typical behavior of VIM for this degree of freedom. The new graphic is presented in Figure 21.

According to Figure 21 the largest yaw amplitudes occur in $Vr \cong 8.0$, a very similar result to that usually related for VIM in the transverse direction.

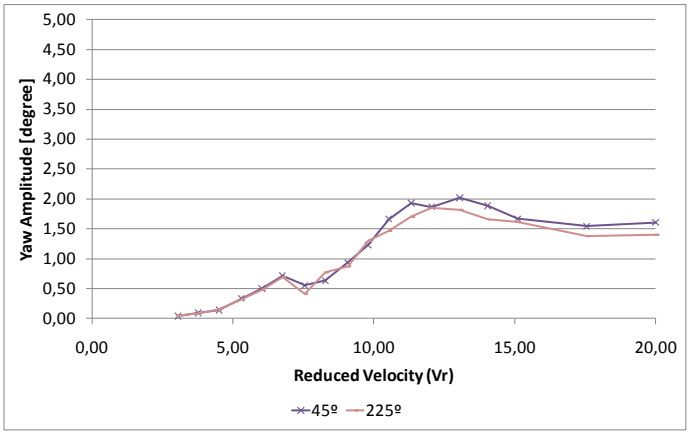

Figure 20 – Yaw characteristic amplitudes for different current incidences: 45 and 225 degrees.

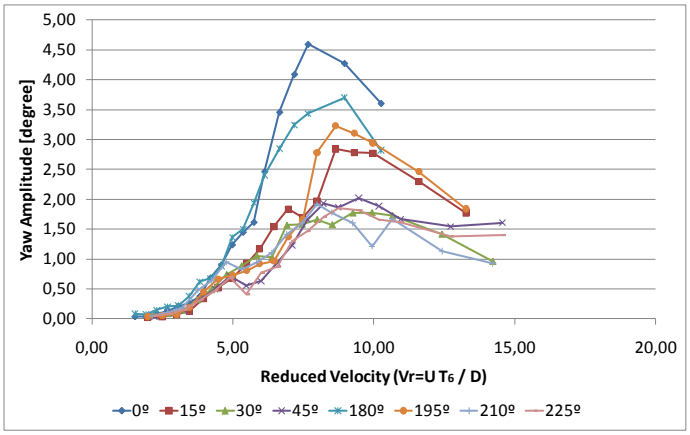

Figure 21 – Yaw characteristic amplitudes for different current incidences: 0, 15, 30, 45, 180, 195, 210 and 225 degrees; as a function of corrected reduced velocity ($Vr = UT_6/D$), where T_6 is natural period of the yaw motion in still waters.

4.4. Time History and Motions in the XY Plane

Results in the XY plane and example of time history are presented in this section in order to better understand the VIM of the semi-submersible.

Figure 22 presents the time history for 45 degree incidence and $Vr = 3.78$. This reduced velocity corresponds to a region before lock-in starts for the motions in the transverse direction. In this condition, the transverse motion has a dominant oscillation frequency.

Figure 23 presents the time history for 45 degree incidence and $Vr = 6.76$. This reduced velocity corresponds to the peak of oscillation in the lock-in region for the transverse motion. The motions in the transverse direction present a well defined oscillation frequency and large amplitudes, $A_y/L \cong 0.4$. The yaw motion, even at small oscillation amplitudes, begins to exhibit oscillations with a frequency similar to the transverse ones.

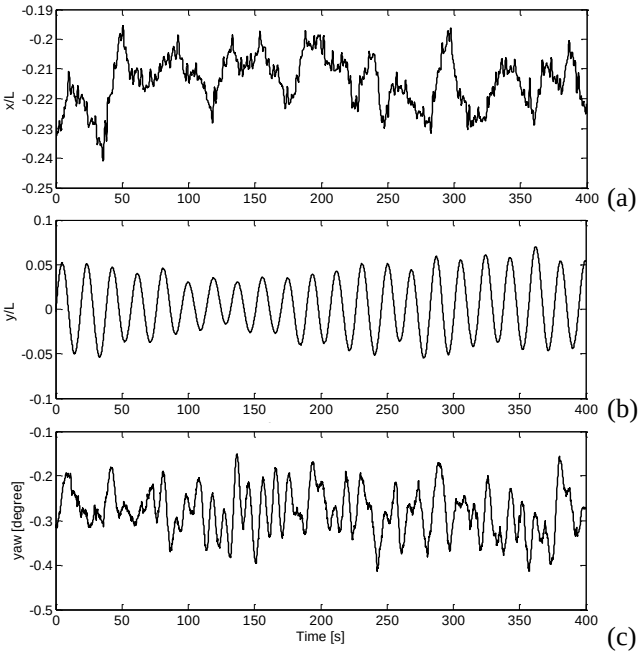

Figure 22 – Example of time history for $Vr = 3.78$ and 45-deg incidence for the motions: (a) in-line direction, (b) transverse direction, and (c) yaw.

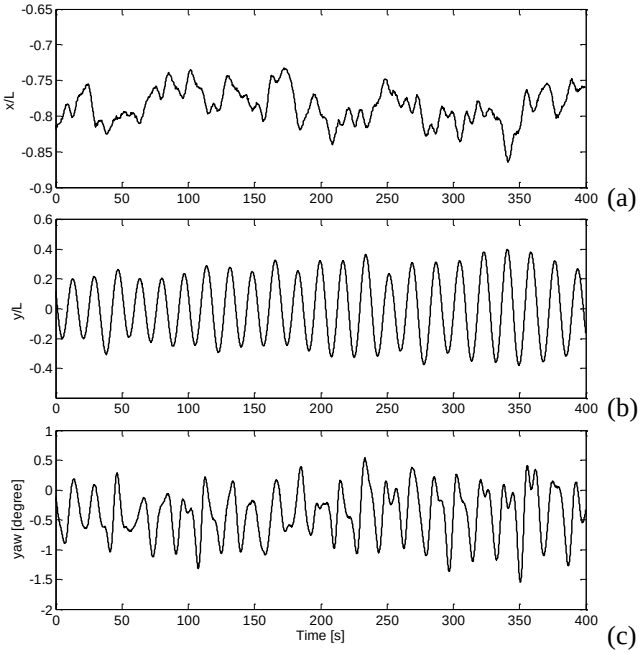

Figure 23 – Example of time history for $Vr = 6.76$ and 45-deg incidence for the motions: (a) in-line direction, (b) transverse direction, and (c) yaw.

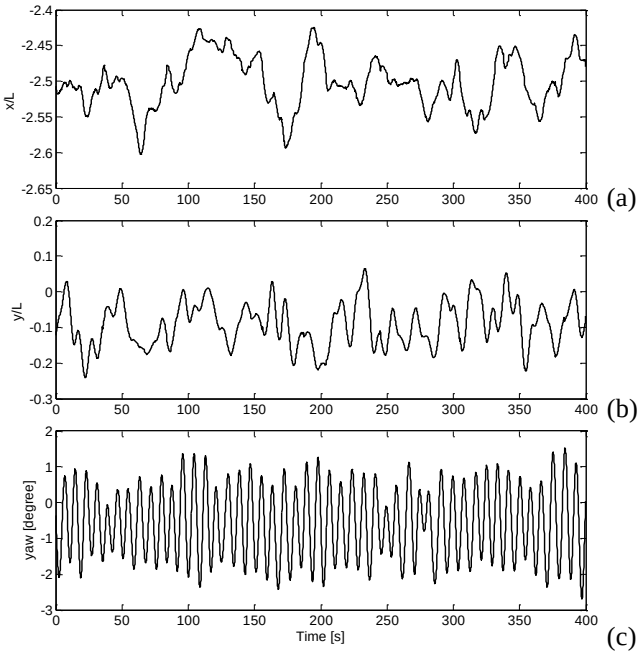

Figure 24 – Example of time history for $Vr = 12.06$ and 45-deg incidence for the motions: (a) in-line direction, (b) transverse direction, and (c) yaw.

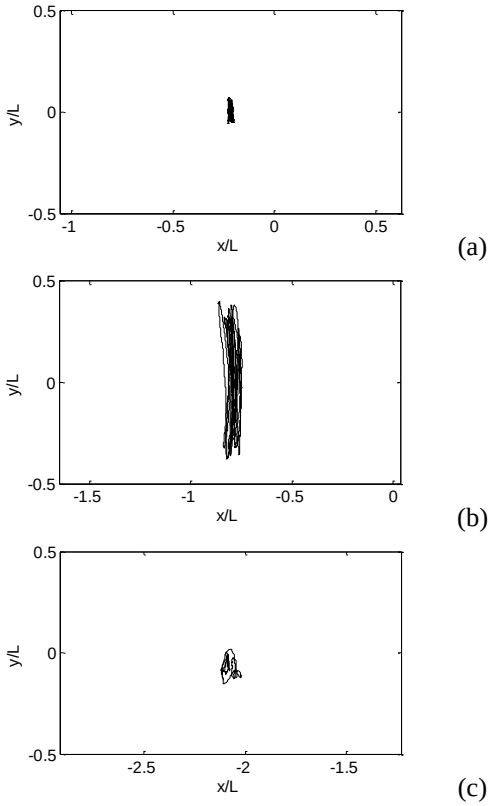

Figure 25 – Example of the motions in the XY plane for 45-deg incidence for different reduced velocity: (a) $Vr = 3.78$, (b) $Vr = 6.76$, and (c) $Vr = 12.06$.

Complementarily, Figure 24 presents the time history for 45 degree incidence and $Vr = 12.06$. This reduced velocity corresponds to the peak of yaw motions, i.e. in the yaw lock-in region. It is interesting to note that in this reduced velocity the transverse and in-line motions do not present a characteristic periodicity but the frequency of the yaw motions is clearly defined.

Finally, for the same 45 degree incidence and the same reduced velocities ($Vr = 3.78$, $Vr = 6.76$ and $Vr = 12.06$), the motions in the XY plane are presented in Figure 25. According to the results, there are no eight-shaped trajectories as those typically presented in spar and monocolumn VIM.

5. GENERAL CONCLUSIONS

The influence of the current incidence angles on VIM of a semi-submersible was discussed. The experimental results were presented for a small-scale model (1:100). The main results discussed comply with motions in the transverse and in-line direction, as well as with the vortex-induced yaw motion (VIY).

The following conclusions can be presented:

1. The largest VIM in the transverse direction was observed for 30, 45, 210 and 225 degrees;
2. In general, the VIM in the transverse direction occurs in a range of $4.0 \leq Vr \leq 14.0$ with peaks around $7.0 \leq Vr \leq 8.0$. The largest amplitudes obtained were $A_y/L \cong 0.4$;
3. The experimental results showed that the hard pipes were the hull appendages which had great influence in the VIM response of the semi-submersible. The 0 and 180 degrees incidences showed the largest difference between them;
4. The motions in the in-line direction were presented in the range of $.0 \leq Vr \leq 10.0$ for all incidence conditions, but with small amplitudes $A_x/L < 0.15$ and peak in $V_r \cong 6$;
5. Although the largest amplitudes in the transversal and in-line direction occur in the same time, the motions in the XY plane did not present an eight-shaped trajectory;
6. Considerable yaw motion oscillations were verified in these tests. A lock-in region could be identified as vortex-induced yaw motions (VIY);
7. The largest yaw motions were verified for the 0 and 180 degree incidences and the maxima amplitudes, in degrees, around $A \cong 4.5$.

NOMENCLATURE

ω	Instantaneous frequency
$\emptyset$	Incidence current angle
A	Characteristic yaw motion amplitude
A_x/L	Nondimensional characteristic motion amplitude in the in-line direction

A_y/L	Nondimensional characteristic motion amplitude in the transverse direction
D	Characteristic length of the section of the body subjected to a vortex shedding
L	Face dimension of the column
U	Incident current velocity
V_r	Reduced velocity
T_0	Natural period of the motion in the transverse direction in still water
T_6	Natural period of the yaw motion in still water

ACKNOWLEDGMENTS

The authors thank PETROBRAS for the financial support to the tests hereby presented. A special acknowledgment to the Oceânica Offshore – Brazil personnel, especially Eng. Marcos Cueva, for the help in the model tests at IPT.

REFERENCES

1. Gonçalves, R. T., Franzini, G. R., Rosetti, G. F., Fujarra, A. L. C., & Nishimoto, K. (2010). *"Analysis Methodology of Vortex-Induced Motions (VIM) on a Monocolumn Platform Applying the Hilbert-Huang Transform Method"*. 29th International Conference on Ocean, Offshore and Arctic Engineering. Shanghai, China: OMAE2010-20101.
2. Gonçalves, R. T., Rosetti, G. F., Franzini, G. R., Fujarra, A. L., & Nishimoto, K. (2010). *"Case Study of Vortex-Induced Motions (VIM) on a Monocolumn Platform Applying the Hilbert-Huang Transform Method"*. 20th International Offshore (Ocean) and Polar Engineering Conference. Beijing, China: ISOPE-2010-TPC-144.
3. Hong, Y., Choi, Y., Lee, J., & Kim, Y. (2008). *"Vortex-Induced Motion of a Deep-Draft Semi-Submersible in Current and Waves"*. 18th International Offshore and Polar Engineering Conference. Vancouver, BC, Canada.
4. Huang, N. E., Shen, Z., Long, S. R., Wu, M. C., Shih, H. H., Zheng, Q., Yen, N-C., Tung, C. C., & Liu, H. H. (1998). *"The Empirical Mode Decomposition and the Hilbert Spectrum for Nonlinear and Non-stationary Time Series Analysis"*. Proceedings of the Royal Society London A, pp. 903-995.
5. Rijken, O., Leverette, S., & Davies, K. (2004). *"Vortex Induced Motions of Semi Submersible with Four Square Columns"*. 16th Deep Offshore Technology Conference and Exhibition. New Orleans, Louisiana, USA.
6. Rijken, O., & Leverette, S. (2008). *"Experimental Study into Vortex Induced Motion Response of Semi Submersilble with Square Columns"*. 27th International Conference on Offshore Mechanics and Arctic Engineering. Estoril, Portugal: OMAE2008-57396.
7. Rijken, O., & Leverette, S. (2009). *"Field Measurements of Vortex Induced Motions of a Deep Draft Semisubmersible"*. 28th International Conference on Ocean, Offshore and Arctic Engineering. Honolulu, Hawaii, USA: OMAE2009-79803.
8. Stansberg, C. T. (2008). *"Current Effects on a Moored Floating Platform in a Sea State"*. 27th International Conference on Offshore Mechanics and Arctic Engineering. Estoril, Portugal: OMAE2008-57621.
9. Xiang, S., Cao, P., Rijken, O., Ma, J., & Chen, Y. (2010). *"Riser VIM Fatigue Design Induced by Deep Draft Semi-Submersible"*. 29th International Conference on Ocean, Offshore and Arctic Engineering. Shanghai, China: OMAE2010-20339.
10. Waals, O. J., Phadke, A. C., & Bultema, S. (2007). *"Flow Induced Motions of Multi Column Floaters"*. 26th International Conference on Offshore Mechanics and Arctic Engineering. San Diego, California, USA: OMAE2007-29539.